The ISME Journal (2011) 5, 305–316

www.nature.com/ismej

ORIGINAL ARTICLE

Genome-scale dynamic modeling of the competition between *Rhodoferax* and *Geobacter* in anoxic subsurface environments

Kai Zhuang[1], Mounir Izallalen[2], Paula Mouser[2], Hanno Richter[2], Carla Risso[2], Radhakrishnan Mahadevan[1] and Derek R Lovley[2]

[1]*Department of Chemical Engineering and Applied Chemistry, Institute of Biomaterials and Biomedical Engineering, University of Toronto, Toronto, Ontario, Canada and* [2]*Department of Microbiology, University of Massachusetts, Amherst, MA, USA*

The advent of rapid complete genome sequencing, and the potential to capture this information in genome-scale metabolic models, provide the possibility of comprehensively modeling microbial community interactions. For example, *Rhodoferax* and *Geobacter* species are acetate-oxidizing Fe(III)-reducers that compete in anoxic subsurface environments and this competition may have an influence on the *in situ* bioremediation of uranium-contaminated groundwater. Therefore, genome-scale models of *Geobacter sulfurreducens* and *Rhodoferax ferrireducens* were used to evaluate how *Geobacter* and *Rhodoferax* species might compete under diverse conditions found in a uranium-contaminated aquifer in Rifle, CO. The model predicted that at the low rates of acetate flux expected under natural conditions at the site, *Rhodoferax* will outcompete *Geobacter* as long as sufficient ammonium is available. The model also predicted that when high concentrations of acetate are added during *in situ* bioremediation, *Geobacter* species would predominate, consistent with field-scale observations. This can be attributed to the higher expected growth yields of *Rhodoferax* and the ability of *Geobacter* to fix nitrogen. The modeling predicted relative proportions of *Geobacter* and *Rhodoferax* in geochemically distinct zones of the Rifle site that were comparable to those that were previously documented with molecular techniques. The model also predicted that under nitrogen fixation, higher carbon and electron fluxes would be diverted toward respiration rather than biomass formation in *Geobacter*, providing a potential explanation for enhanced *in situ* U(VI) reduction in low-ammonium zones. These results show that genome-scale modeling can be a useful tool for predicting microbial interactions in subsurface environments and shows promise for designing bioremediation strategies.

The ISME Journal (2011) **5,** 305–316; doi:10.1038/ismej.2010.117; published online 29 July 2010
Subject Category: integrated genomics and post-genomics approaches in microbial ecology
Keywords: *Geobacter*; *Rhodoferax*; community modeling; bioremediation; systems microbiology

Introduction

A wide phylogenetic diversity of microorganisms that are capable of dissimilatory metal reduction has been recovered from subsurface environments (Lovley *et al.*, 2004; Lovley, 2006). The factors controlling which species predominate in a given subsurface environment are poorly understood, but may have important environmental consequences. For example, some dissimilatory metal-reducing microorganisms, such as those from the *Geobacteraceae* family, are capable of reducing U(VI) to U(IV), which can impact the mobility of uranium in the subsurface (Lovley, 1991, 2001, 2006; Lovley *et al.*, 1993, 2004; Wall and Krumholz, 2006), whereas others do not reduce U(VI) (Lovley *et al.*, 2004; Lovley, 2006). Stimulating dissimilatory metal reduction to promote the reductive precipitation of uranium shows promise as a bioremediation strategy for uranium-contaminated groundwater (Anderson *et al.*, 2003; Vrionis *et al.*, 2005), but relies on stimulating the appropriate dissimilatory metal-reducing microorganisms.

Field studies on *in situ* uranium bioremediation at a uranium-contaminated site in Rifle, CO, have shown that *Rhodoferax* and *Geobacter* species, two phylogenetically distinct groups of dissimilatory metal-reducing microorganisms, are important components of the naturally anoxic subsurface at

Correspondence: R Mahadevan, Department of Chemical Engineering and Applied Chemistry, Institute of Biomaterials and Biomedical Engineering, University of Toronto, 200 College Street Room 326, Toronto, Canada M5S3E5.
E-mail: krishna.mahadevan@utoronto.ca
Received 14 January 2010; revised 14 June 2010; accepted 17 June 2010; published online 29 July 2010

this site (Mouser *et al*., 2009). Multiple field experiments at the Rifle site have shown that when dissimilatory metal reduction is artificially stimulated with the addition of acetate to the subsurface, *Geobacter* consistently become the predominant dissimilatory Fe(III) reducing microorganisms (Holmes *et al*., 2002, 2007; Anderson *et al*., 2003; Chang *et al*., 2005; Wilkins *et al*., 2009). This is despite the fact that similar to *Geobacter* species (Lovley *et al*., 1993, 2004; Caccavo *et al*., 1994), the one described Fe(III)-reducing *Rhodoferax* species, *Rhodoferax ferrireducens*, is also capable of oxidizing acetate with the reduction of Fe(III) (Finneran *et al*., 2003). In contrast to the *Geobacter* species, *R. ferrireducens* has not been shown to be capable of U(VI) reduction, and cannot fix nitrogen in the absence of ammonium (Figure 1b; Finneran *et al*., 2003). Therefore, the ability of *Geobacter* species to outcompete *Rhodoferax* species may be critical to the success of stimulated *in situ* bioremediation at the Rifle site, and presumably other similar uranium-contaminated environments. The relative

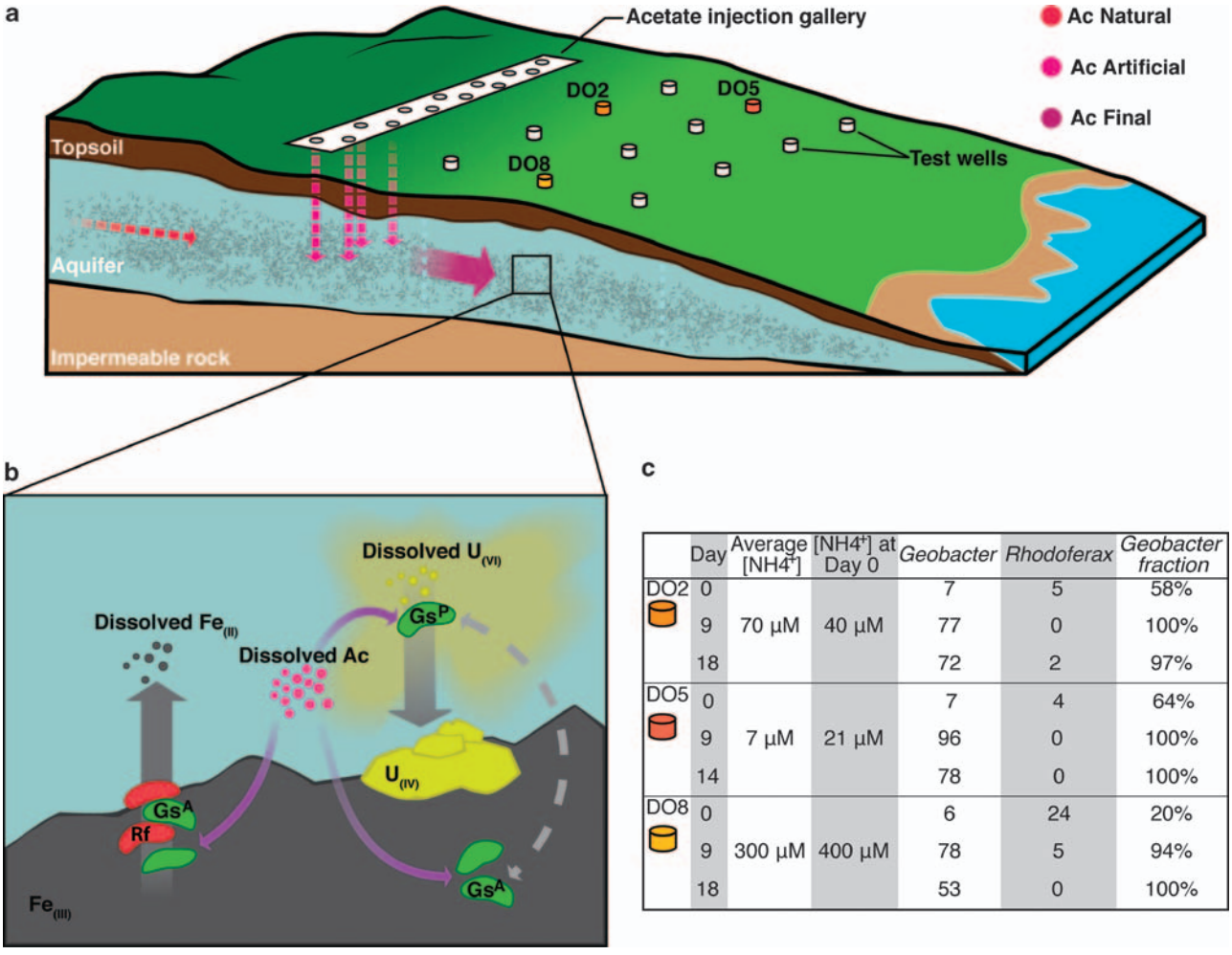

	Day	Average [NH4+]	[NH4+] at Day 0	*Geobacter*	*Rhodoferax*	*Geobacter* fraction
DO2	0			7	5	58%
	9	70 μM	40 μM	77	0	100%
	18			72	2	97%
DO5	0			7	4	64%
	9	7 μM	21 μM	96	0	100%
	14			78	0	100%
DO8	0			6	24	20%
	9	300 μM	400 μM	78	5	94%
	18			53	0	100%

Figure 1 Conceptual model of uranium bioremediation. (**a**) Before acetate injection, acetate is generated in the subsurface primarily through fermentation. During bioremediation, acetate is injected to the subsurface at high concentrations through the injection galleries. The artificial flow of acetate is combined with natural acetate flow, and follows the direction of the ground water. This acetate stimulates the growth of multiple microbial species downstream of the injection galleries, including *Geobacter* and *Rhodoferax* species. Groundwater samples are collected periodically at the test wells downstream of the injection galleries, including wells D02, D05 and D08. Various tests were performed on these groundwater samples, including ammonium concentration measurements and 16S rRNA-based analysis of the relative microbial abundance (Mouser *et al*. 2009). (**b**) Both *Geobacter* and *Rhodoferax* oxidize the dissolved acetate, and carry out the reduction of Fe(III) by attaching to a Fe(III) surface. *Geobacter* is also capable of reducing U(VI) in its planktonic phase. Given that Fe(III) is the primary electron acceptor for *Geobacter*, this implies that the organisms compete for both electron donor and acceptor. The reduction of Fe(III) creates dissolved Fe(II), whereas the reduction of dissolved U(VI) creates U(IV), which precipitates. The reductive precipitation of uranium effectively removes uranium from the groundwater. Abbreviations: Rf, Rhodoferax; GsA, *Geobacter* (attached to sediment); GsP, *Geobacter* (planktonic). (**c**) Ammonium concentrations at wells D02, D05 and D08 have been measured periodically (Mouser *et al*., 2009) Here, the initial and average ammonium concentrations are shown. The *Geobacter* and *Rhodoferax* columns show the number of *Geobacter* and *Rhodoferax* 16S *rRNA* genes as a percentage of the total genes in the sample. The *Geobacter* fraction is calculated using equation (1). The relative abundance of these two organisms seems to be related to the concentration of ammonium.

abundance of *Rhodoferax* and *Geobacter* species in different subsurface locations within the site has been measured and suggests that the competition among these Fe(III) reducers is related, at least in part, to the availability of ammonium in those locations (Figure 1c) (Mouser *et al.*, 2009).

Constraint-based metabolic models (Fell and Small, 1986; Watson, 1986; Varma and Palsson, 1994) offer the possibility of predicting the physiological responses of microorganisms to a diversity of environmental conditions, as well as the interactions of microorganisms with each other and their environments (Lovley, 2003; Scheibe *et al.*, 2009). Flux balance analysis is a constraint-based modeling technique that is able to predict metabolic fluxes in microorganisms under different growth conditions without information on the kinetic parameters for each individual metabolic reaction (Feist and Palsson, 2008; Oberhardt *et al.*, 2009). Genome-scale flux balance analysis models of pure cultures, such as *Escherichia coli* (Ibarra *et al.*, 2002; Reed and Palsson, 2003; Reed *et al.*, 2003; Feist *et al.*, 2007; Feist and Palsson, 2008) and *Geobacter* species (Mahadevan *et al.*, 2006; Segura *et al.*, 2008; Sun *et al.*, 2009), are capable of predicting the detailed physiology including growth yields and respiration rates. This modeling approach has been useful for both understanding the behavior of biological systems in complex environments and for engineering purposes (Burgard *et al.*, 2003; Pharkya *et al.*, 2003, 2004; Pharkya and Maranas, 2006; Hjersted *et al.*, 2007; Anesiadis *et al.*, 2008; Izallalen *et al.*, 2008). The availability of the genome sequences of *Geobacter* (Methe *et al.*, 2003; Sun *et al.*, 2009) and *Rhodoferax* (Risso *et al.*, 2009) species provides the opportunity to apply genome-scale modeling techniques to examine the interaction and competition between *Geobacter* and *Rhodoferax* species under naturally occurring and artificially stimulated Fe(III)-reducing conditions.

It has been previously shown that it is possible to model the syntrophic growth of two microorganisms with a small-scale metabolic model (Stolyar *et al.*, 2007). However, in that model, the stoichiometric matrices of the two partners, *Desulfovibrio vulgaris* and *Methanococcus maripaludis*, were coupled directly and dynamic changes in the biomass concentrations of the individual species were not considered. Although this approach may be appropriate when the microorganisms are interdependent, it is inappropriate in ecological settings where the community composition is dynamic. To predict metabolic behavior of such microbial systems, in which other interactions—such as competition—are important, we have developed the dynamic multi-species metabolic modeling (DMMM) framework based on the dynamic flux balance analysis (Mahadevan *et al.*, 2002). The advantages of the DMMM framework over a Monod kinetics-based model and the model of Stolyar *et al.* are discussed in more detail in the Supplementary Information.

In this paper, we present a dynamic metabolic model of *Geobacter sulfurreducens* and *R. ferrireducens*, implemented using the DMMM framework (Figure 2), and show how this approach can provide important insights into the factors controlling the relative abundance of *Geobacter* and *Rhodoferax* species under different subsurface conditions. This is the first model to dynamically integrate multiple genome-scale metabolic models.

Materials and methods

The dynamic multi-species metabolic modeling framework

We have developed the DMMM framework, a computational framework capable of integrating multiple pre-existing genome-scale metabolic models into a community metabolic model. The DMMM framework was used to integrate the previously published models of *G. sulfurreducens* and *R. ferrireducens* into a community model of subsurface iron-reducers (Figure 2). The formulation and implementation of the DMMM framework is described in detail in the Supplementary Information.

Modeling resource availability

In anoxic sedimentary environments, complex organic matter is fermented with acetate as the primary fermentation product (Lovley and Phillips, 1989; Lovley and Chapelle, 1995; Lovley *et al.*, 2004). Thus, the slow steady release of acetate from fermentation is expected to be the primary natural source of acetate in the subsurface sediments at the Rifle site.

The rates of microbial processes have been studied in various organics-poor sediments. In a Danish shallow sandy aquifer similar to the Rifle aquifer, the rate of acetate oxidation associated with iron-reduction, sulfate-reduction and methanogenesis was reported to be between 0 and 0.5 $\mu M\,h^{-1}$ (Hansen *et al.*, 2001). Similar values have been reported for oligotrophic lake, marine and salt marsh sediments (Crill and Martens, 1986) reported that the acetate turnover rate in a methane-producing marine sediment to be 0.40 $\mu M\,h^{-1}$ at 30 cm depth. Kuivila *et al.* (1989) reported that the acetate production rate from fermentation was between 0.035 and 0.17 $\mu M\,h^{-1}$. Balba and Nedwell (1982) reported that the acetate utilization rate in salt marsh sediment is in the range of 0–4.8 $\mu M\,h^{-1}$. Lovley and Klug (1983) reported that the total rate of microbial metabolism in a lake sediment to be 6.4 $\mu M\,h^{-1}$, which provides an upper limit for the acetate turnover in that environment. In a previous sediment model, Lovley and Klug (1986) have assumed 3 $\mu M\,h^{-1}$ to be the rate of acetate turnover in oligotrophic sediments. The acetate turnover rate in a deep aquifer is measured to be 0.0135 $\mu M\,h^{-1}$ at 35 m depth (Chapelle and Lovley, 1990), which is assumed to be the lower bound for

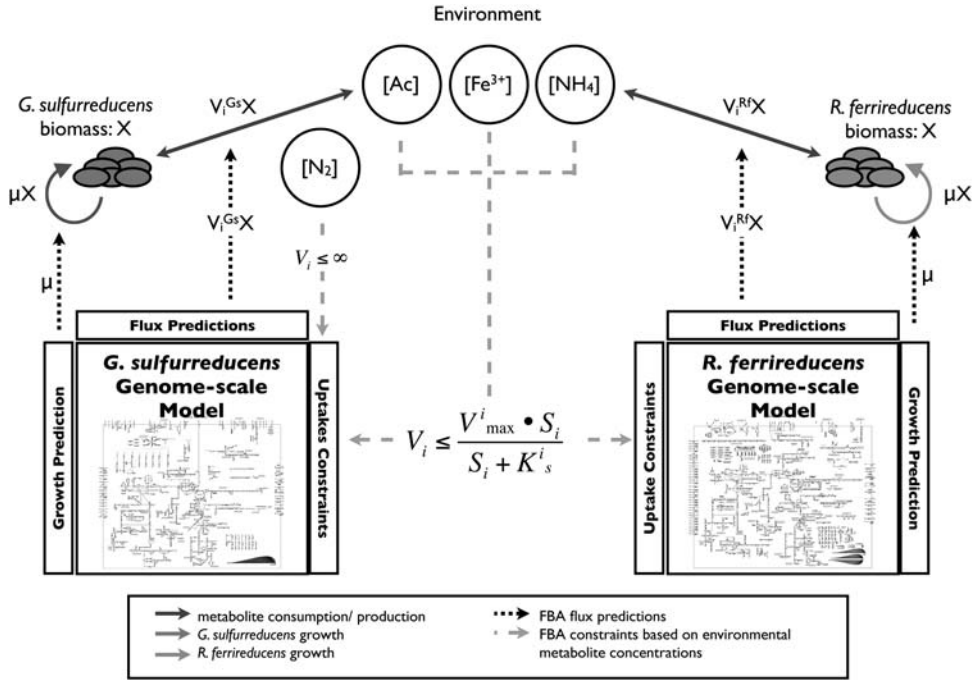

Figure 2 DMMM of *Geobacter* and *Rhodoferax* community. The *in silico* representation of a minimal community whose growth depends on the oxidation of acetate coupled to Fe(III) reduction. Here, μ is the biomass growth rate, V_i^{Gs} is the flux of metabolite, i predicted by the *G. sulfurreducens* model (Mahadevan *et al.* 2006), V_i^{Rf} is the flux of metabolite, i predicted by the *R. ferrireducens* model (Risso *et al.* 2009), X is the biomass concentration, $[S_i]$ is the concentration of i^{th} metabolite, K_s^i is the saturation constant for i^{th} metabolite. The simulations in this paper assume the field to be a spatial homogeneous chemostat to simplify the transport and geochemical process.

our simulations. On the basis of these previous findings, we assumed the acetate flux into the subsurface at Rifle is between 0 to 0.54 μM h^{-1} before the stimulation of metabolism through the addition of acetate.

The ammonium concentrations were set to range from 5 to 400 μM, which correspond to the ammonium concentrations previously observed at the Rifle site (Mouser *et al.*, 2009).

Previous sediment sampling at bioremediation sites reported that the Fe(III) concentration to be in the range of 5–40 μMol g^{-1} of sediment (Anderson *et al.*, 2003; Vrionis *et al.*, 2005; Yabusaki *et al.*, 2007; Komlos *et al.*, 2008), which includes both microbially reducible Fe(III) and Fe(III) that is resistant to reduction. If it is assumed that the sediment density is 2 g ml^{-1} (Petrie *et al.*, 2003) and that ~50% of Fe(III) is bioavailable, then 2.5–20 mmol of Fe(III) per liter of groundwater is available for microbial reduction. Therefore, the initial Fe(III) concentration was assumed to be 10 mmol per liter for both pre-injection and during-injection simulations.

The initial cell density for both *G. sulfurreducens* and *R. ferrireducens* were assumed to be 10^5 cells l^{-1} based on previous results for the Rifle site (Holmes *et al.*, 2007). The average cell mass of *G. sulfurreducens* is experimentally measured to be 10^{-12} g $cell^{-1}$ (Izallalen *et al.*, 2008). On the basis of the volume ratio between *G. sulfurreducens* and *R. ferrireducens*, and assuming their intracellular contents have a similar physical density, the average cell mass of *R. ferrireducens* is calculated to be 6.25×10^{-12} g $cell^{-1}$ (see Supplementary Information). Recent studies have shown that a high proportion of *Geobacter* species do not firmly attach to subsurface sediments at the Rifle site (Strycharz *et al.*, 2009) and therefore, it was assumed that cells were planktonic and that the biomass was fully affected by dilution due to groundwater flow.

The simulations model the field as a spatially homogeneous chemostat, which simplifies the transport and geochemical process. The groundwater flow in the subsurface is modeled using a dilution rate of 0.034 day^{-1}, or 0.0014 h^{-1} (see Supplementary Information for calculation). As this study was not designed to model field-scale events, we focused solely on community competition dynamics. However, efforts are underway to integrate this dynamic community model with a reactive transport model of the Rifle site similar to a previously described method (Scheibe *et al.*, 2009).

The injection of acetate to promote U(VI) reduction at the Rifle site results in acetate concentrations of 3–5 mM (Anderson *et al.*, 2003; Vrionis *et al.*, 2005). The acetate injection rate was calculated by multiplying the acetate concentration of 3 mM by the dilution rate, resulting in an acetate flux of 0.0042 mM h^{-1}. This value was used to simulate the acetate flux during acetate injection. As the measured ammonium concentrations *in situ* did not change significantly during the course of

bioremediation, the ammonium concentration during acetate amendment was fixed at 400 μM for the ammonium-excess simulation and fixed at 5 μM for the ammonium-limiting simulation. The parameters used in the simulation are summarized in the Supplementary Information.

Treatment of experimental data and model assessment
Data from the 2007 field experiment at Rifle, CO (Mouser *et al.*, 2009) were used to assess the accuracy of the community dynamics predicted by the model. These data include the initial and average ammonium concentrations, as well as the *in situ* abundance of 16S rRNA of *G. sulfurreducens* and *R. ferrireducens* before the start of the acetate injection (day 0) and 9, 14, 18 days after the start of the injection (Figure 1c). To compare the relative abundance of *Geobacter* and *Rhodoferax* species mathematically, we defined a metric called the '*Geobacter* fraction' (equation (1)). A higher *Geobacter* fraction value indicates a greater abundance of *Geobacter* species relative to *Rhodoferax*. Both 16S rRNA abundance (experimentally measured using reverse transcription-quantitative PCR; Mouser *et al.*, 2009) and computationally predicted cell densities were converted to *Geobacter* fraction value using equation (1).

$$\text{Geobacter fraction} = \frac{\text{No. of } G.\ sulfurreducens}{\text{No. of } G.\ sulfurreducens + \text{No. of } R.\ ferrireducens} \quad (1)$$

The prediction accuracy of the model was accessed for both natural conditions and during injection conditions by comparing simulated *Geobacter* fractions with experimental *Geobacter* fractions at test wells D02, D05 and D08. For both cases, the ammonium concentrations were set to the measured concentrations before acetate injection at these wells.

Results and Discussion

Community competition under natural conditions
Before addition of acetate to the groundwater, fermentation of complex organic matter is expected to be the primary source of acetate to *Rhodoferax* and *Geobacter* species. The rate of this natural supply of acetate at the Rifle site is not known, but is expected to fall within the range of acetate turnover rates that have been observed in various sedimentary environments (Crill and Martens, 1986; Lovley and Klug, 1986; Kuivila *et al.*, 1989; Chapelle and Lovley, 1990; Hansen *et al.*, 2001). The steady-state *Geobacter* fractions generated using low acetate turnover rates of 0.2, 0.25 and 0.38 $\mu M\,h^{-1}$ were compared with the *Geobacter* fraction values calculated from experimental measurement at day 0 (Figure 3). This comparison suggests that the acetate turnover rates are close to 0.2 $\mu M\,h^{-1}$ at well D02, 0.38 $\mu M\,h^{-1}$ at well D05 and 0.25 $\mu M\,h^{-1}$ at well D08 (Figure 3). All three inferred acetate turnover rates fall within the range measured in similar environments (Figure 3; Chapelle and Lovley, 1990; Hansen *et al.*, 2001). These results also suggest that this model could be used to predict the community dynamics under natural conditions more accurately if measurements of the acetate turnover rates at the three wells before injection were available.

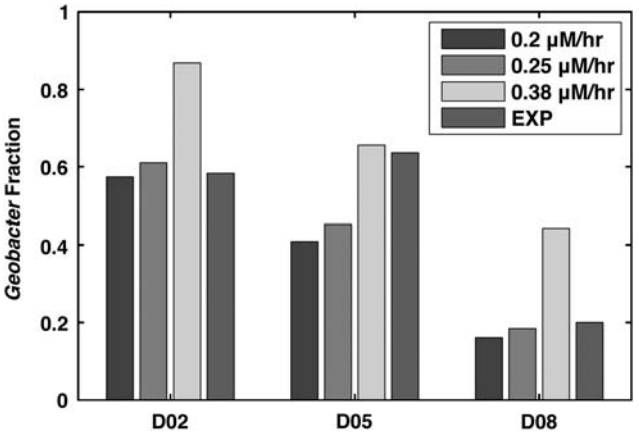

Figure 3 Comparison between predicted and measured *Geobacter* fractions under natural conditions. Predicted *Geobacter* fractions at D02, D05 and D08 before the acetate addition are generated using acetate turnover rates of 0.2, 0.25 and 0.38 $\mu M\,h^{-1}$. The predictions are compared with the *Geobacter* fraction values calculated from experimental 16S rRNA measurements at the respective wells, at day 0 (Mouser *et al.* 2009). This comparison suggests that the acetate turnover rates are close to 0.2 $\mu M\,h^{-1}$ at well D02, close to 0.38 $\mu M\,h^{-1}$ at well D05, and close to 0.25 $\mu M\,h^{-1}$ at well D08. All three inferred acetate turnover rates fall within the range measured in similar environments, which supports the predicted competition dynamics at natural conditions.

The community competition was simulated over three different (low, medium and high) acetate turnover ranges (Figure 4). The simulations suggest that at low acetate turnover rates, *Rhodoferax* species are likely to be more abundant than *Geobacter* species, especially when ammonium is in excess. This prediction is consistent with the results of the analysis of 16S *rRNA* gene sequences at the Rifle site before the addition of acetate (Mouser *et al.*, 2009).

Risso *et al.*, 2009 analyzed the energetics of *R. ferrireducens* by comparing predicted yields with experimental yields under multiple conditions, and found that the proton translocation stoichiometry at cytochrome reductase of $2H^+/2e^-$ was consistent with the data for *R. ferrireducens*, whereas the stoichiometry at cytochrome reductase that could explain experimental data was found to be $1H^+/2e^-$ for *G. sulfurreducens* (Mahadevan *et al.*, 2006). The doubling of cytochrome reductase energetic efficiency led to a significant increase in the efficiency of the electron transport chain and the

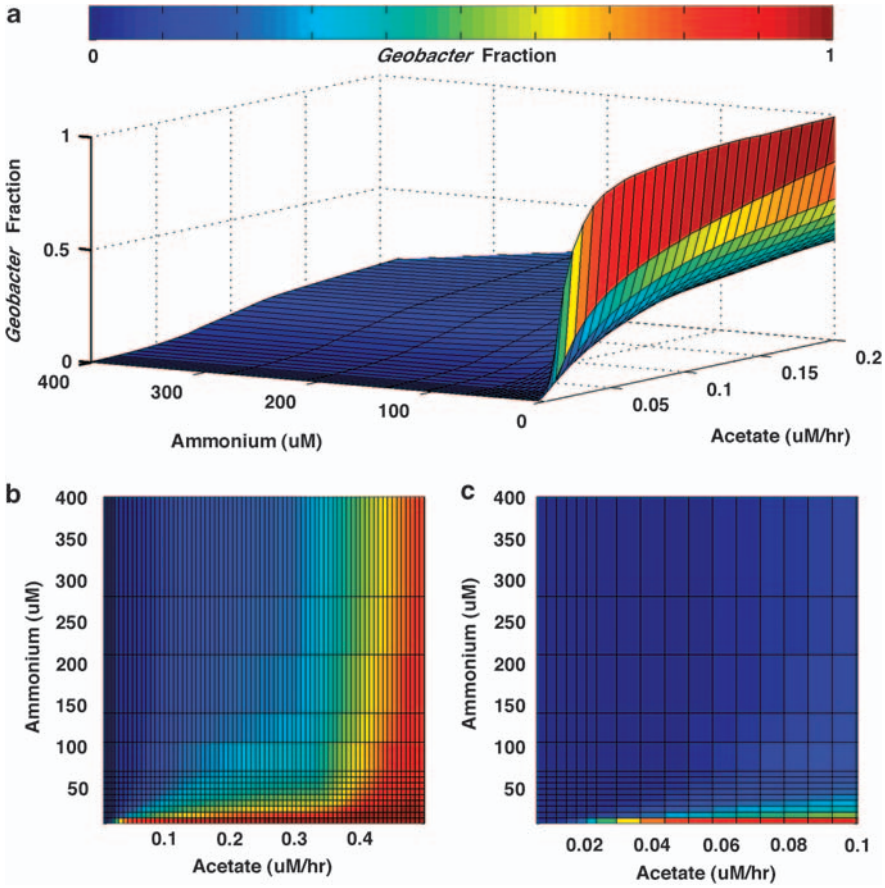

Figure 4 Relative composition of *Geobacter* and *Rhodoferax* in Fe(III) reducing community before acetate amendment. The steady-state community compositions at three different acetate turnover rate ranges are simulated. The *Geobacter* fraction is used to measure the relative success of *Geobacter* to *Rhodoferax* species. The competition with respect to the ammonium concentration and acetate turnover rate is viewed at three different scales with respect to the acetate turnover rate. (**a**) The acetate turnover rates range from 0 to 0.2 $\mu M\,h^{-1}$. At this scale, the nonlinearity of the competition is highlighted. (**b**) The acetate turnover rates range from 0 to 0.54 $\mu M\,h^{-1}$, corresponding to the range of subsurface acetate availability reported by Hansen *et al.* (2001). (**c**) The acetate turnover rates range from 0 to 0.1 $\mu M\,h^{-1}$, corresponding to the rates measured in an aquifer extremely poor in acetate (Chapelle and Lovley, 1990).

predicted *Rhodoferax* biomass yield during Fe(III) respiration. Model simulations show that under acetate-limited growth on Fe(III), the yield of *R. ferrireducens* is 0.0798 $gDW\,mmol^{-1}$ of acetate, nearly two times the yield of *G. sulfurreducens* (0.0437 $gDW\,mmol^{-1}$ of acetate). Thermodynamic analysis of cellular growth shows that the free energy of substrate oxidation can either be used to drive metabolic reactions at higher rates or to produce biomass; in other words, an organism can either optimize for substrate uptake rate or optimize for energetic efficiency (Pfeiffer *et al.*, 2001; Pfeiffer and Bonhoeffer, 2003, 2004; Pfeiffer and Schuster, 2005; Schuster *et al.*, 2008). Therefore, by choosing to optimize for efficiency, *Rhodoferax* has a higher biomass yield at the expense of growth rate, resulting in a significantly lower substrate uptake rate compared with *Geobacter*. This is exemplified by the observation that the maximum acetate uptake rate of *G. sulfurreducens* (18 $mmol\,gDW^{-1}\,h^{-1}$) is more than 10-fold higher than that of *R. ferrireducens* (1.71 $mmol\,gDW^{-1}\,h^{-1}$).

It was previously shown that yield strategists are favored over rate strategists under low substrate flux conditions (Pfeiffer *et al.*, 2001). The same rationale can be applied to the anoxic Fe(III)-reducing microbial community. The growth rate is the product of the substrate uptake rate and yield ($\mu = V_s \times Y$). At low acetate turnover conditions, the low environmental acetate flux limits the uptake rate of *Geobacter* to a fraction of its maximum. If both organisms have similar uptake rates, then the growth rate of *Rhodoferax* will be significantly higher, as its yield is twice that of *Geobacter*. This explains the abundance of *Rhodoferax* at low acetate turnover conditions when ammonium is readily available (Figure 4c). As acetate turnover rate increases, the acetate no longer limits growth. When the acetate turnover rate is sufficiently high to allow *Geobacter* uptake rates to become more than two times that of *Rhodoferax*, the growth rate of *Geobacter* becomes greater than that of *Rhodoferax*. Therefore, *Geobacter* becomes more competitive at higher acetate fluxes (Figures 4a and b).

The modeling suggests that the availability of ammonium in the sediments also has a major role in the relative abundance of *Geobacter* and *Rhodoferax* under natural conditions in the sediments, with *Geobacter* favored at low ammonium conditions (Figures 3 and 4). The community composition varied nonlinearly with respect to ammonium concentration and acetate turnover rate (Figure 4a). The region of coexistence (*Geobacter* fraction between 0.4 and 0.6) of *Rhodoferax* and *Geobacter* under steady-state conditions was narrow; minute changes in acetate and ammonium fluxes led to the complete dominance of one organism (Figures 4b and c). The simulations predicted that as the availability of ammonium decreased, *Geobacter* would become more competitive with *Rhodoferax* at lower acetate turnover rates (Figure 4). This can be attributed to the ability of *Geobacter* to fulfill its nitrogen requirements from fixation of nitrogen, whereas *Rhodoferax* is incapable of nitrogen fixation. Availability of acetate in excess, results in the limitation in ammonium for *Rhodoferax*, favoring the growth of *Geobacter*. A high expression of genes for nitrogen fixation in *Geobacter* species living in a diversity of subsurface sediments (Holmes *et al.*, 2004, 2007; Mouser *et al.*, 2009), has suggested that they are actively involved in nitrogen fixation in the subsurface. *Geobacter* nitrogen fixation genes may even be expressed when low ($<50\,\mu M$) concentrations are available in sediments (Holmes *et al.*, 2009), suggesting that such subsurface sediments may well contain microzones that are ammonium depleted. The presence of such microzones would further facilitate the coexistence of *Geobacter* and *Rhodoferax*, with growth of *Geobacter* favored in the ammonium-depleted microzones. However, the current model does not incorporate spatial heterogeneity and therefore cannot predict such spatial variations in community composition.

The insights derived from our simulations can be applied to understand the competition between *Geobacter* and *Rhodoferax* in other environments. For example, *Geobacter* is found to dominate in a landfill leachate-contaminated Dutch aquifer with high ammonium content (Lin *et al.*, 2007). In this case, the leachate contamination contains 50–100 $mg\,l^{-1}$ of dissolved organic carbon (Lin *et al.*, 2007), which is much higher than the natural dissolved organic carbon content at the Rifle site ($<5\,mg\,l^{-1}$; Barlett, Personal Communication). Therefore, the leachate contamination itself provides a rich organic nutrient source, presumably leading to an increased rate of acetate production through fermentation in the Dutch aquifer relative to that of Rifle. The increase in the acetate production rate favors the rate optimizing *Geobacter* species, leading to their dominance.

Community competition when acetate is added to the subsurface

Our simulation predictions of the community composition during the acetate addition at wells

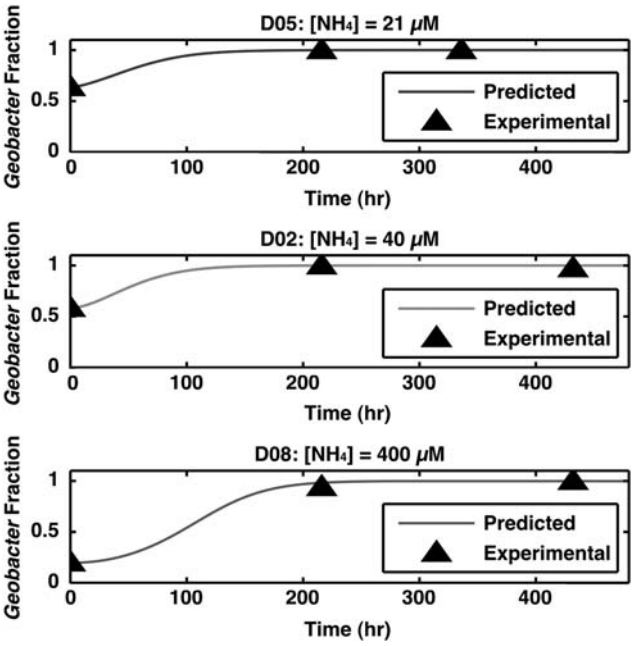

Figure 5 Comparison between predicted and measured *Geobacter* fractions during acetate addition. The predicted *Geobacter* fractions at wells D02, D05 and D08 are compared with the experimentally measured fractions at the respective wells. Simulations are initiated with the *Geobacter* fractions and ammonium concentrations measured at day 0 in wells D02 (58%, 40 μM), D05 (64%, 21 μM) and D08 (20%, 400 μM) (Mouser *et al.* 2009). The predicted *Geobacter* fractions (solid lines) are compared with the *Geobacter* fractions calculated from the experimental 16S rRNA measurements (▲).

D02, D05 and D08 show the same trend as the values calculated from the 16S rRNA measurements (Figure 5). These simulations (Figure 5) agree with previous observations that the addition of millimolar concentrations of acetate to the subsurface to stimulate *in situ* uranium bioremediation at the Rifle site significantly influences the relative proportions of *Geobacter* and *Rhodoferax*, with *Geobacter* species consistently becoming the predominant microorganisms regardless of ammonium availability (Anderson *et al.*, 2003; Vrionis *et al.*, 2005; Holmes *et al.*, 2007; Mouser *et al.*, 2009). Furthermore, the predicted number of *Geobacter* cells is within an order of magnitude relative to the measured number of *Geobacter* cells at day 19 (Figure 6; Holmes *et al.*, 2007).

The reasons for this were readily apparent from the dynamic genome-scale modeling (Figure 6). Here, the acetate injection rate was calculated to be 4.2 $\mu M\,h^{-1}$ based on the assumed geometry (Anderson *et al.*, 2003; Vrionis *et al.*, 2005). At this acetate flux, the ammonium flux in the ammonium excess case (estimated by multiplying the dilution rate and the steady ammonium concentration to be 0.56 $\mu M\,h^{-1}$) is more than sufficient for biomass synthesis and is not limiting. In the ammonium limiting case, the ammonium flux (0.035 $\mu M\,h^{-1}$) is

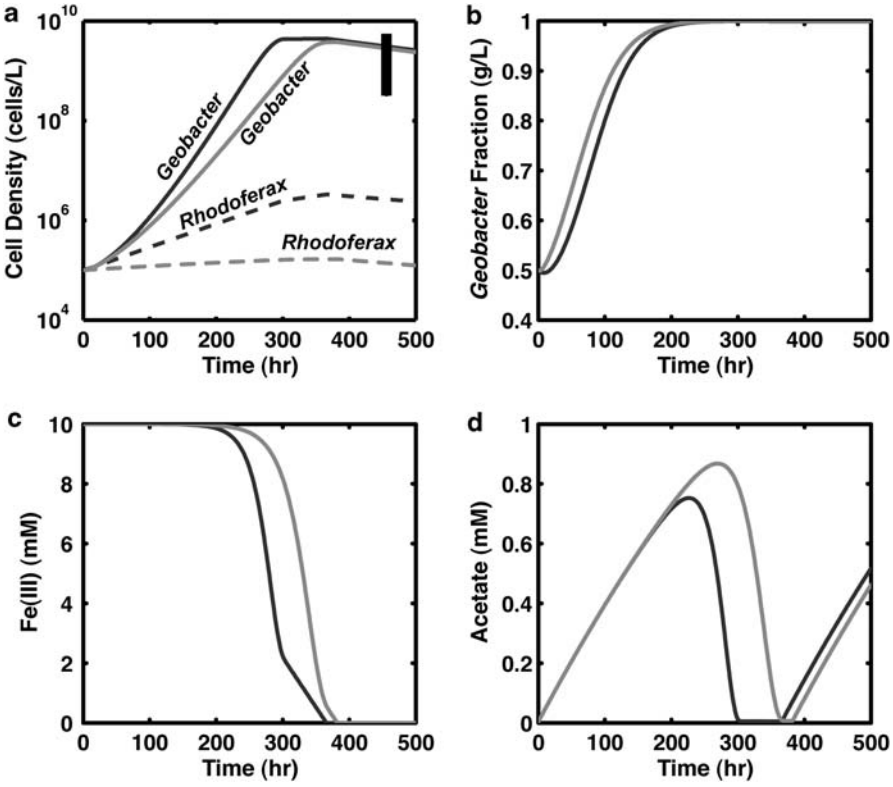

Figure 6 Simulation of the competition dynamics in a Fe(III)-reducing community during acetate addition. Biomass concentrations of *G. sulfurreducens* and *R. ferrireducens* (**a**), *Geobacter* fractions (**b**), acetate concentration (**c**) and Fe(III) concentration (**d**) under both ammonium-limiting and ammonium-excess conditions are shown. Under both conditions, *Geobacter* outcompetes *Rhodoferax* soon after acetate addition begins. The blue lines are the ammonium-excess simulation results; the red lines are the ammonium-limiting simulation results. The black bar in (**a**) represents the experimentally measured range of the *Geobacter* cell density at day 19 (Holmes *et al.*, 2007). Simulations are initialized with equal concentrations of *Geobacter* and *Rhodoferax*. The acetate injection rate of 3 mM day^{-1} (4.2 μM h^{-1}) is used for both ammonium-limiting ((ammonium) = 0.005 mM) and ammonium-excess conditions ((ammonium) = 0.4 mM). Note: the *y* axis of (**a**) is in log scale, whereas the *y* axis of (**b**, **c** and **d**) are in linear scale.

a primary limitation of growth at the same level of acetate availability. *Geobacter* rapidly responded to increased acetate availability with a substantial increase in biomass, whether or not sufficient ammonium was available to completely support all of the acetate-dependent growth (Figures 6a and b). In contrast, the growth rate of *R. ferrireducens* was just above the dilution rate in the ammonium excess case, whereas there is a loss in *Rhodoferax* biomass in the ammonium limiting case. This reflects the absolute requirement (Figures 6a and b) of ammonium to support the growth of *Rhodoferax*. Low ammonium delayed, but did not prevent extensive growth of *Geobacter*. However, the maximum amount of *Geobacter* biomass was lower under ammonium-limiting conditions because of the increased energetic demands for nitrogen fixation (Figure 6a). With extended time, Fe(III) was depleted and *Geobacter* declined (Figures 6a and c). The acetate concentration is briefly reduced to zero before rising again after the occurrence of Fe(III) depletion under both conditions (Figure 6d).

The high flux of acetate from the artificial addition allows both species to achieve their maximum acetate uptake rate. As the maximum acetate uptake rate of *Geobacter* is more than 10 times higher than that of *Rhodoferax*, whereas the yield of *Rhodoferax* is only twice higher than that of *Geobacter*, the growth rate of *Geobacter* is significantly higher than that of *Rhodoferax* when both organisms use acetate at their respective maximum uptake rates. Therefore, during bioremediation, *Geobacter*'s advantage in uptake rate outweighs *Rhodoferax*'s advantage in yield, leading to the overwhelming success of *Geobacter*.

The cell densities and the Fe(III) concentration before acetate injection can vary greatly in the field before acetate amendment. To evaluate the sensitivity of the competition dynamics to variations in the initial cell densities and Fe(III) concentrations, simulations with different initial Fe(III) concentrations (2.5, 5, 10 and 20 mmol l^{-1}) and cell densities (10^4, 10^5 and 10^6 cells l^{-1}) were performed. These simulations showed no significant changes in the dynamics of the competition, suggesting that the variations in these two parameters would not affect the increase in the *Geobacter* fraction following acetate amendment (data not shown). Despite the lack of spatial and geochemical descriptions in our model, we were able to predict the trend changes

in the community composition; this suggests that biological interactions are perhaps the dominant factor for influencing the microbial ecology in the Rifle subsurface.

Predicted changes in metabolic states and its implications for bioremediation

An additional feature of the genome-scale metabolic models, relative to models based on Monod kinetics with constant yield parameters, is their capability to predict changes in the metabolic states of microorganisms under different environmental conditions. For organisms with few physiological states, traditional models, which depend on experimentally measured yields for each state, are sufficient. As the number of physiological states increase, the complexity of implementing a Monod kinetics-based model increases as additional data for the different physiological states are required and each state has to be addressed individually (see Supplementary Information). When acetate is the donor, the metabolism of *Rhodoferax* is relatively simple and can be modeled with traditional methods, but *Geobacter* has many physiological states, such as acetate-limiting ammonium utilization mode, iron-limiting ammonium utilization mode, acetate-limiting nitrogen fixation mode and iron-limiting nitrogen fixation mode, which require constraint-based models to predict. The genome-scale model predicted that the biomass yields of *Geobacter* can vary between 1.95 and 4.05 gDW per mol acetate (Scheibe *et al.*, 2009). Under ammonium-depleted conditions, *R. ferrireducens* is predicted to experience a maintenance phase with no associated growth because of the lack of ammonium, but with the ability to generate ATP by oxidizing acetate coupled to Fe(III) reduction. In contrast, *G. sulfurreducens* is able to grow in the absence of ammonium by nitrogen fixation.

The necessity for nitrogen fixation is predicted to have a number of environmentally relevant physiological consequences for *Geobacter* (Figure 7). The genome-scale model predicts that to meet increased energetic demands associated with nitrogen fixation, more acetate enters the tricarboxylic acid cycle, resulting in higher fluxes through NADH dehydrogenase and extracellular electron transfer, and ATP synthase (Figure 7). Under nitrogen-fixing conditions, less biomass is produced; this is reflected in the increased acetate activation through acetyl-CoA transferase instead of acetate kinase, as well as less pyruvate production through pyruvate oxidoreductase for biomass synthesis. These changes in metabolic fluxes are predicted to result in a 30% reduction in growth yield (Figure 7 and Supplementary Figure S8 in Supplementary Information). A reduction of *Geobacter* biomass yield under nitrogen-fixation conditions has been observed experimentally (Methe *et al.*, 2005).

The predicted shift in metabolism associated with nitrogen fixation could have a significant impact on

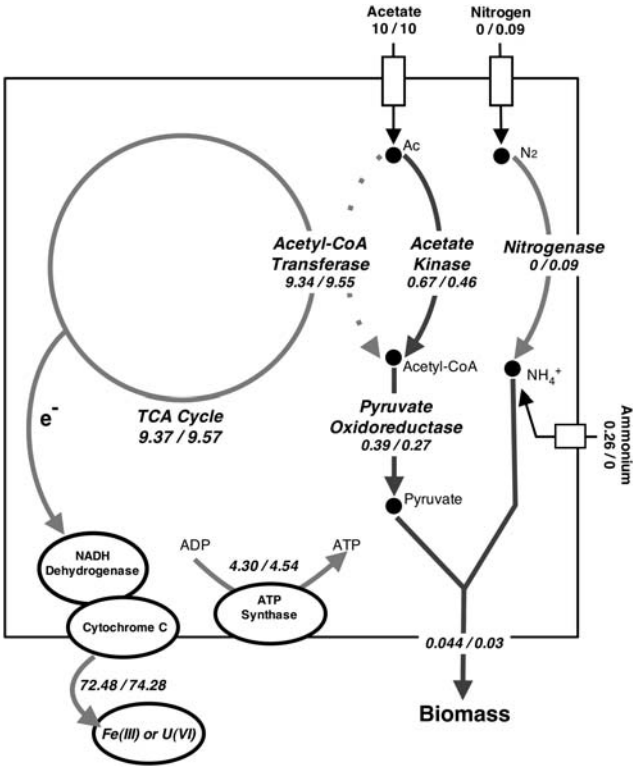

Figure 7 Comparison of the predicted flux distribution during growth with ammonium vs nitrogen-fixation dependent growth of *G. sulfurreducens*. The predicted flux distributions of *G. sulfurreducens* during growth with unlimited ammonium uptake and nitrogen-fixation dependent growth are compared. The biomass flux is measured in h^{-1}; all other fluxes are measured in mmol $gDW^{-1}\,h^{-1}$. The red fluxes are increased during nitrogen fixation; the blue fluxes are decreased during nitrogen fixation. The first number represents the flux through the reaction when ammonium is acquired through environmental uptake; the second number represents the flux through the reaction when ammonium is provided through nitrogen fixation.

the effectiveness of *in situ* uranium bioremediation. The rate of U(VI) reduction depends on both the specific uranium reduction rate and the biomass concentration. During nitrogen fixation, the rate of U(VI) reduction per cell may increase because of the up-regulation of respiration, at the expense of biomass production. This prediction of the model is consistent with field results at the Rifle site. In the 2007 field experiment, U(VI) was much more effectively removed from the groundwater at sites low in ammonium than at sites with relatively high-ammonium concentrations (Mouser *et al.*, 2009). This trade-off between the specific uranium reduction rate and the biomass yield can be evaluated using the DMMM framework, and it may be possible with dynamic optimization techniques to predict from genome-scale metabolic models the optimal ammonium concentrations for maximal rates of U(VI) reduction. This would be analogous to the recent design of a *G. sulfurreducens* strain with increased respiration rates and lower biomass yields

using genome-scale metabolic modeling (Izallalen *et al.*, 2008).

Implications

The simulations suggest that *Geobacter* and *Rhodoferax* species have adopted very different strategies for growth in subsurface environments. *Geobacter* sacrificed maximizing yield from substrate utilization in favor of rapid growth and the ability to grow in the absence of ammonium, whereas *Rhodoferax* are more optimized for higher growth yields. Both strategies seem to be adaptive for growth under natural subsurface conditions at the Rifle site. *Geobacter* and *Rhodoferax* are found within the same sampling zones. This probably reflects the growth of *Geobacter* and *Rhodoferax* species in different microenvironments within the heterogeneous subsurface environment. The ability of *Geobacter* to grow faster than *Rhodoferax* at high acetate concentrations and to multiply in the absence of ammonium permits it to rapidly respond to the artificial conditions imposed when acetate is added to promote *in situ* uranium bioremediation. It is fortuitous that *Geobacter* outcompete *Rhodoferax* under these conditions, because pure culture studies have suggested that *Geobacter* (Lovley, 1991; Caccavo *et al.*, 1994), but not *Rhodoferax* (Finneran *et al.*, 2003) species are capable of U(VI) reduction. If this distinction were true for all *Rhodoferax* species, then *in situ* uranium reduction would be much less effective if *Rhodoferax* could readily compete with *Geobacter* under high acetate/low ammonium conditions.

There are other microbial interactions that are likely to impact the effectiveness of *in situ* uranium bioremediation. Most notably, the consumption of added acetate by acetate-oxidizing sulfate reducers that are ineffective in U(VI) reduction (Anderson *et al.*, 2003) may limit U(VI) reduction by *Geobacter* species, decreasing the efficacy of the bioremediation (Anderson *et al.*, 2003; Vrionis *et al.*, 2005). As genome-scale models for these sulfate reducers become available, it should be possible to evaluate this interaction in a manner similar to that reported here for *Geobacter*/*Rhodoferax* interactions. Furthermore, the increasing availability of the genome sequences of environmentally relevant microorganisms should make it feasible to apply genome-scale metabolic modeling to further investigate the ecology of a wide diversity of microbial ecosystems.

Acknowledgements

This research was supported by the Office of Science (BER), the US Department of Energy, Cooperative Agreement No. DE-FC02-02ER63446 and Grant No. DE-FG02-07ER64367; this research was also supported by the Canada Foundation for Innovation and the University of Toronto Open Fellowship, as well as the Government of Canada through Genome Canada and the Ontario Genomics Institute (2009-OGI-ABC-1405). We thank Caitlin O'Connel for her artistic illustration, Laurence Yang for his insightful discussions and Emma Janssen for her grammatical corrections.

References

Anderson RT, Vrionis HA, Ortiz-Bernad I, Resch CT, Long PE, Dayvault R *et al.* (2003). Stimulating the *In Situ* activity of *Geobacter* species to remove uranium from the groundwater of a uranium-contaminated aquifer. *Appl Environ Microbiol* **69**: 5884–5891.

Anesiadis N, Cluett WR, Mahadevan R. (2008). Dynamic metabolic engineering for increasing bioprocess productivity. *Metab Eng* **10**: 255–266.

Balba MT, Nedwell DB. (1982). Microbial metabolism of acetate, propionate and butyrate in anoxic sediment from the Colne Point Saltmarsh, Essex, UK. *J Gen Microbiol* **128**: 1415–1422.

Burgard AP, Pharkya P, Maranas CD. (2003). Optknock: a bilevel programming framework for identifying gene knockout strategies for microbial strain optimization. *Biotechnol Bioeng* **84**: 647–657.

Caccavo F, Lonergan DJ, Lovley DR, Davis M, Stolz JF, McInerney MJ. (1994). *Geobacter sulfurreducens* sp. nov., a hydrogen- and acetate-oxidizing dissimilatory metal-reducing microorganism. *Appl Environ Microbiol* **60**: 3752–3759.

Chang YJ, Long PE, Geyer R, Peacock AD, Resch CT, Sublette K *et al.* (2005). Microbial incorporation of 13C-labeled acetate at the field scale: detection of microbes responsible for reduction of U(VI). *Environ Sci Technol* **39**: 9039–9048.

Chapelle FH, Lovley DR. (1990). Rates of microbial metabolism in deep coastal plain aquifers. *Appl Environ Microbiol* **56**: 1865–1874.

Crill PM, Martens CS. (1986). Methane production from bicarbonate and acetate in an anoxic marine sediment. *Geochim Cosmochim Acta* **50**: 2089–2097.

Feist AM, Henry CS, Reed JL, Krummenacker M. (2007). A genome-scale metabolic reconstruction for *Escherichia coli* K-12 MG1655 that accounts for 1260 ORFs and thermodynamic information. *Mol Syst Biol* **3**: 121.

Feist AM, Palsson B. (2008). The growing scope of applications of genome-scale metabolic reconstructions using *Escherichia coli*. *Nat Biotechnol* **26**: 659–667.

Fell DA, Small JR. (1986). Fat synthesis in adipose tissue. An examination of stoichiometric constraints. *Biochem J* **238**: 781–786.

Finneran KT, Johnsen CV, Lovley DR. (2003). *Rhodoferax ferrireducens* sp. nov., a psychrotolerant, facultatively anaerobic bacterium that oxidizes acetate with the reduction of Fe(III). *Int J Syst Evol Microbiol* **53**: 669–673.

Hansen LK, Jakobsen R, Postma D. (2001). Methanogenesis in a shallow sandy aquifer, Rømø, Denmark. *Geochimica et Cosmochimica Acta* **65**: 2925–2935.

Hjersted JL, Henson MA, Mahadevan R. (2007). Genome-scale analysis of *Saccharomyces cerevisiae* metabolism and ethanol production in fed-batch culture. *Biotechnol Bioeng* **97**: 1190–1204.

Holmes DE, Bond DR, O'Neil RA, Reimers CE, Tender LR, Lovley DR. (2004). Microbial communities associated with electrodes harvesting electricity from a variety of aquatic sediments. *Microb Ecol* **48**: 178–190.

Holmes DE, Finneran KT, O'Neil RA, Lovley DR. (2002). Enrichment of members of the family *Geobacteraceae* associated with stimulation of dissimilatory metal reduction in uranium-contaminated aquifer sediments. *Appl Environ Microbiol* **68**: 2300–2306.

Holmes DE, O'Neil RA, Chavan MA, N'Guessan LA, Vrionis HA, Perpetua LA *et al.* (2009). Transcriptome of *Geobacter uraniireducens* growing in uranium-contaminated subsurface sediments. *ISME J* **3**: 216–230.

Holmes DE, O'Neil R, Vrionis HA, N'guessan L, Ortiz-Bernad I, Larrahondo MJ *et al.* (2007). Subsurface clade of Geobacteraceae that predominates in a diversity of Fe(III)-reducing subsurface environments. *ISME J* **1**: 663–677.

Ibarra RU, Edwards JS, Palsson BO. (2002). *Escherichia coli* K-12 undergoes adaptive evolution to achieve *in silico* predicted optimal growth. *Nature* **420**: 186–189.

Izallalen M, Mahadevan R, Burgard A, Postier B, Didonato R, Sun J *et al.* (2008). *Geobacter sulfurreducens* strain engineered for increased rates of respiration. *Metab Eng* **10**: 267–275.

Komlos J, Peacock A, Kukkadapu RK, Jaffé PR. (2008). Long-term dynamics of uranium reduction/reoxidation under low sulfate conditions. *Geochim Cosmochim Acta* **72**: 3603–3615.

Kuivila KM, Murray JW, Devol AH, Novelli PC. (1989). Methane production, sulfate reduction and competition for substrates in the sediments of Lake Washington. *Geochim Cosmochim Acta* **53**: 409–416.

Lin B, Braster M, Röling WFM, van Breukelen BM. (2007). Iron-Reducing Microorganisms in a Landfill Leachate-Polluted Aquifer: Complementing Culture-Independent Information with Enrichments and Isolations. *Geomicrobiol J* **24**: 283–294.

Lovley DR. (1991). Dissimilatory Fe(III) and Mn(IV) reduction. *Microbiol Rev* **55**: 259–287.

Lovley DR. (2001). Bioremediation. *Anaerobes to the rescue Science* **293**: 1444–1446.

Lovley DR. (2003). Cleaning up with genomics: applying molecular biology to bioremediation. *Nat Rev Microbiol* **1**: 35–44.

Lovley DR. (2006). Dissimilatory Fe(III)- and Mn(IV)-Reducing Prokaryotes. In: (eds). *The Prokaryotes*. Springer: New York, pp 1143.

Lovley DR, Chapelle FH. (1995). Deep subsurface microbial processes. *Rev Geophys* **33**: 365–381.

Lovley DR, Giovannoni SJ, White DC, Champine JE, Phillips EJ, Gorby YA *et al.* (1993). *Geobacter metallireducens gen.* nov. sp. nov., a microorganism capable of coupling the complete oxidation of organic compounds to the reduction of iron and other metals. *Arch Microbiol* **159**: 336–344.

Lovley DR, Holmes DE, Nevin KP. (2004). Dissimilatory Fe(III) and Mn(IV) reduction. *Adv Microb Physiol* **49**: 219–286.

Lovley DR, Klug MJ. (1983). Sulfate reducers can outcompete methanogens at freshwater sulfate concentrations. *Appl Environ Microbiol* **45**: 187–192.

Lovley DR, Klug MJ. (1986). Model for the distribution of sulfate reduction and methanogenesis in freshwater sediments. *Geochim Cosmochim Acta* **50**: 11–18.

Lovley DR, Phillips EJ. (1989). Requirement for a microbial consortium to completely oxidize glucose in Fe(III)-reducing sediments. *Appl Environ Microbiol* **55**: 3234–3236.

Mahadevan R, Bond DR, Butler JE, Esteve-Nuñez A, Coppi MV, Palsson BO *et al.* (2006). Characterization of metabolism in the Fe(III)-reducing organism *Geobacter sulfurreducens* by constraint-based modeling. *Appl Environ Microbiol* **72**: 1558–1568.

Mahadevan R, Edwards JS, Doyle FJ. (2002). Dynamic flux balance analysis of diauxic growth in *Escherichia coli*. *Biophys J* **83**: 1331–1340.

Methe BA, Nelson KE, Eisen JA, Paulsen IT. (2003). Genome of *Geobacter sulfurreducens*: metal reduction in subsurface environments. *Science* **302**: 1967–1969.

Methe BA, Webster J, Nevin K, Butler J, Lovley DR. (2005). DNA microarray analysis of nitrogen fixation and Fe(III) reduction in *Geobacter sulfurreducens*. *Appl Environ Microbiol* **71**: 2530–2538.

Mouser PJ, N'Guessan AL, Elifantz H, Holmes DE, Williams KH, Wilkins MJ *et al.* (2009). Influence of heterogeneous ammonium availability on bacterial community structure and the expression of nitrogen fixation and ammonium transporter genes during *in situ* bioremediation of uranium-contaminated groundwater. *Environ Sci Technol* **43**: 4386–4392.

Oberhardt MA, Palsson BO, Papin JA. (2009). Applications of genome-scale metabolic reconstructions. *Mol Syst Biol* **5**: 320.

Petrie L, North NN, Dollhopf SL, Balkwill DL, Kostka JE. (2003). Enumeration and characterization of iron(III)-reducing microbial communities from acidic subsurface sediments contaminated with uranium(VI). *Appl Environ Microbiol* **69**: 7467–7479.

Pfeiffer T, Bonhoeffer S. (2003). An evolutionary scenario for the transition to undifferentiated multicellularity. *Proceedings of the National Academy of Sciences* **100**: 1095–1098.

Pfeiffer T, Bonhoeffer S. (2004). Evolution of cross—feeding in microbial populations. *Am Nat* **163**: E126–E135.

Pfeiffer T, Schuster S. (2005). Game-theoretical approaches to studying the evolution of biochemical systems. *Trends Biochem Sci* **30**: 20–25.

Pfeiffer T, Schuster S, Bonhoeffer S. (2001). Cooperation and competition in the evolution of ATP-producing pathways. *Science* **292**: 504–507.

Pharkya P, Burgard AP, Maranas CD. (2003). Exploring the overproduction of amino acids using the bilevel optimization framework OptKnock. *Biotechnol Bioeng* **84**: 887–899.

Pharkya P, Burgard AP, Maranas CD. (2004). OptStrain: a computational framework for redesign of microbial production systems. *Genome Res* **14**: 2367–2376.

Pharkya P, Maranas CD. (2006). An optimization framework for identifying reaction activation/inhibition or elimination candidates for overproduction in microbial systems. *Metab Eng* **8**: 1–13.

Reed JL, Palsson B. (2003). Thirteen years of building constraint-based *in silico* models of *Escherichia coli*. *J Bacteriol* **185**: 2692–2699.

Reed JL, Vo TD, Schilling CH, Palsson B. (2003). An expanded genome-scale model of *Escherichia coli* K-12 (iJR904 GSM/GPR). *Genome Biol* **4**: R54.

Risso C, Sun J, Zhuang K, Mahadevan R, DeBoy R, Ismail W *et al.* (2009). Genome-scale comparison and constraint-based metabolic reconstruction of the facultative anaerobic Fe(III)-reducer *Rhodoferax ferrireducens*. *BMC Genomics* **10**: 447.

Scheibe TD, Mahadevan R, Fang Y, Garg S. (2009). Coupling a genome-scale metabolic model with a reactive transport model to describe *in situ* uranium bioremediation. *Microb Biotechnol* **2**: 274–286.

Schuster S, Pfeiffer T, Fell DA. (2008). Is maximization of molar yield in metabolic networks favoured by evolution? *J Theor Biol* **252**: 497–504.
Segura D, Mahadevan R, Juárez K, Lovley DR. (2008). Computational and experimental analysis of redundancy in the central metabolism of *Geobacter sulfurreducens*. *PLoS Comput Biol* **4**: e36.
Stolyar S, Van Dien S, Hillesland KL, Pinel N, Lie TJ, Leigh JA *et al.* (2007). Metabolic modeling of a mutualistic microbial community. *Mol Syst Biol* **3**: 92.
Strycharz A, Peacock A, Williams KH, N'Guessan L, Lovley DR. (2009). *Geobacter* species are predominately planktonic during growth in uranium-contaminated subsurface sediments. *American Society for Microbiolgy 109th General Meeting* **14**: 447.
Sun J, Sayyar B, Butler JE, Pharkya P, Fahland TR, Famili I *et al.* (2009). Genome-scale constraint-based modeling of *Geobacter metallireducens*. *BMC Syst Biol* **3**: 15.
Varma A, Palsson BO. (1994). Stoichiometric flux balance models quantitatively predict growth and metabolic by-product secretion in wild-type *Escherichia coli* W3110. *Appl Environ Microbiol* **60**: 3724–3731.
Vrionis HA, Anderson RT, Ortiz-Bernad I, Ortiz-Bernad I, O'Neil KR, Resch CT *et al.* (2005). Microbiological and geochemical heterogeneity in an *in situ* uranium bioremediation field site. *Appl Environ Microbiol* **71**: 6308–6318.
Wall JD, Krumholz LR. (2006). Uranium reduction. *Annu Rev Microbiol* **60**: 149–166.
Watson MR. (1986). A discrete model of bacterial metabolism. *Comput Appl Biosci* **2**: 23–27.
Wilkins MJ, Verberkmoes NC, Williams KH, Callister SJ, Mouser PJ, Elifantz H *et al.* (2009). Proteogenomic monitoring of Geobacter physiology during stimulated uranium bioremediation. *Appl Environ Microbiol* **75**: 6591–6599.
Yabusaki SB, Fang Y, Long PE, Resch CT, Peacock AD, Komlos J *et al.* (2007). Uranium removal from groundwater via *in situ* biostimulation: field-scale modeling of transport and biological processes. *J Contam Hydrol* **93**: 216–235.

Appendix

Mathematical symbols

μ	Specific growth rate ($g\,g^{-1}\,h^{-1}$)
r^D	Specific death rate ($g\,g^{-1}\,h^{-1}$)
c^T	FBA objective column: this column chooses which reaction flux(es) is the target of optimization. The most common choice is maximization of biomass flux.
A	The stoichiometric matrix representation of the chemical reaction network
V_i^j	The specific consumption/production rate of the i^{th} metabolite in the environment because of the actions of the j^{th} microbial species ($mmol\,gDW^{-1}\,h^{-1}$)
v	The vector of reaction fluxes ($mmol\,gDW^{-1}h^{-1}$)
v^{max}	The vector of maximum reaction fluxes ($mmol\,gDW^{-1}\,h^{-1}$)
v^{min}	The vector of minimum reaction fluxes ($mmol\,gDW^{-1}\,h^{-1}$)
i	The i^{th} metabolite in the environment
j	The j^{th} organisms of the community
S_i	The concentration of the i^{th} metabolite in the environment
q^S	Uptake rate of substrate S ($mmol\,gDW^{-1}\,h^{-1}$)
m^S	Maintenance requirement of substrate S ($mmol\,gDW^{-1}\,h^{-1}$)
Y	Biomass yield ($gDW\,mmol^{-1}$)
m^{ATP}	Non-growth-related ATP maintenance flux ($mmol\,gDW^{-1}\,h^{-1}$)
$V_{i,max}$	Maximum specific uptake rate of metabolite i ($mmol\,gDW^{-1}\,h^{-1}$)

Abbreviation: FBA, flux balance analysis.

Supplementary Information accompanies the paper on The ISME Journal website (http://www.nature.com/ismej)